Response clustering in transient stochastic synchronization and desynchronization of coupled neuronal bursters

Alexander B. Neiman
Department of Physics and Astronomy and Quantitative Biology Institute, Ohio University, Athens, Ohio 45701, USA
Center for Neurodynamics, University of Missouri at St. Louis, St. Louis, Missouri 63121 USA

David F. Russell* and Tatyana A. Yakusheva†
Center for Neurodynamics, University of Missouri at St. Louis, St. Louis, Missouri 63121 USA

Andrew DiLullo
Department of Physics and Astronomy, Ohio University, Athens, Ohio 45701, USA

Peter A. Tass‡
Institute of Medicine, Virtual Institute of Neuromodulation, Research Center Jülich D-52425, Germany;
Department of Stereotaxy and Functional Neurosurgery, University of Cologne, Cologne D-50931, Germany;
and Brain Imaging Center West, Jülich D-52425, Germany

(Received 17 November 2006; revised manuscript received 12 April 2007; published 8 August 2007)

We studied the transient dynamics of synchronized coupled neuronal bursters subjected to repeatedly applied stimuli, using a hybrid neuroelectronic system of paddlefish electroreceptors. We show experimentally that the system characteristically undergoes poststimulus transients, in which the relative phases of the oscillators may be grouped in several clusters, traversing alternate phase trajectories. These signature transient dynamics can be detected and characterized quantitatively using specific statistical measures based on a stochastic approach to transient oscillator responses.

DOI: 10.1103/PhysRevE.76.021908 PACS number(s): 87.19.La, 05.45.Xt, 05.40.Ca, 87.17.Nn

I. INTRODUCTION

Synchronization is a fundamental phenomenon of rhythm adjustment in systems of coupled nonlinear self-sustained oscillators (for a recent review, see [1,2]). The majority of studies on synchronization have addressed steady states. However, in many applications, including in neuroscience and medicine, the impact of external time-localized perturbations on synchronized oscillators are of primary interest. For example, transient synchronization of neurons is believed to play a crucial role in the processing of sensory information [3–5], and transient synchronization has recently been suggested as a collective mechanism of spatiotemporal integration in the central nervous system [6]. Transient time-localized brain responses evoked by sensory stimuli play a key role in the study of information processing in the brain. For example, in Ref. [7] the effect of phase precession of θ oscillations in the hippocampus was assessed by means of an analysis of the transient synchronization in response to brief stimuli. Transient synchronization in the auditory cortex was recently studied in Ref. [8]. The role of ongoing brain rhythms, especially of a phase reset of neuronal rhythms, in the generation of sensor-evoked brain responses, is still a matter of debate [9].

On the other hand, human neurological disorders such as essential tremor and tremor caused by Parkinson disease or multiple sclerosis appear to be caused by abnormal synchronization of the activity of neuronal populations, departing from the incoherent firing of these neurons under normal conditions [10,11]. Recent studies have shown that this abnormal synchronization is transient, or nonstationary [12]. To improve the empirically derived deep brain stimulation [13], several stimulation procedures were proposed to destroy unwanted synchronization by utilizing either localized pulse stimulation [14,15] or delayed feedback [16,17] (for a recent review, see [18]). Thus, transient synchronization and desynchronization is an important issue in the design of new stimulation procedures.

The dynamics of stimulus-locked transient processes in coupled oscillators was recently studied using numerical models of phase oscillators with instantaneous [19–21] or delayed coupling [22] in the presence of noise. An important prediction from the simulations was that phase resetting stimuli delivered to two oscillators at appropriately chosen times may cause the oscillators' ensemble of transient responses to split into different groups [19]. That is, a perturbed system of coupled oscillators may follow two or more different transient paths as it returns to its original state of synchronization. This response clustering occurs if the coordinated phase resetting stimuli shift the system of coupled oscillators to a particular volume of the phase space from where—after stimulus offset—the trajectories relax toward the stable synchronized state via two different paths [19,22]. In the case of instantaneous coupling (i.e., coupling without delay), the two oscillators have to be reset close to an un-

*Current address: Department of Biological Sciences, Ohio University, Athens, OH 45701, USA
†Current address: Department of Anatomy and Neurobiology, Washington University School of Medicine, 660 Euclid Avenue, St. Louis MI 63121, USA.
‡Author to whom correspondence should be addressed.

stable fixed point of their relative phase [19]. These predictions require validation in a well-defined experimental system of coupled oscillators. For instance, analyses of phase models are restricted to the cases of weak coupling and small perturbations [23]. In fact, it is by no means self-evident that the phase reduction approach is also valid in the case of strong shocklike pulses and subsequent transient oscillator responses [24].

We have developed a well-defined experimental system that utilizes pairs of electroreceptors of paddlefish, which are externally supplied with feedback, and/or coupled, using electronic circuits and real-time computation, to set up synchronized periodic bursting firing patterns of the two electroreceptors' output neurons (afferents, sending action potentials to the brain). Periodic bursting is a widespread type of neuronal activity [25], both normally as well as in disorders such as Parkinson disease [26]. Based on the dynamic clamp approach hybrid neuroelectronic systems [27] were used to study steady-state synchronization of electrically coupled *in vitro* neurons [28,29] and phase resetting curves of single neurons [24]. In this paper, we used small networks of coupled electroreceptors to experimentally study the transient desynchronization and resynchronization dynamics of coupled bursting neurons in an *in vivo* preparation. We present experimental evidence of clustering of transient phase responses in a neural system, confirming predictions from simulations. Also, we demonstrate explicitly the necessity of using specific indices to quantify transient phase resetting data, compared to traditional types of data analysis used widely in neuroscience. The structure of the paper is as follows. In Sec. II, we review stimulus-locked transient dynamics of coupled self-sustained oscillators and introduce measures of transient synchronization. Section III describes paddlefish electroreceptors and experimental methods. Experimental results are described in Sec. IV, followed by conclusions in Sec. V.

II. STIMULUS-LOCKED TRANSIENT DYNAMICS OF COUPLED PHASE OSCILLATORS AND STOCHASTIC PHASE RESETTING ANALYSIS

A. Model for coupled phase oscillators

Let us consider two coupled noisy phase oscillators with natural frequencies $\omega_{1,2}$. We assume that the dynamics of oscillators are captured by their instantaneous phases $\phi_{1,2}(t)$, given by [19]

$$\dot{\phi}_k = \omega_k - \frac{K}{2}\sin(\phi_k - \phi_j) + s_k(t,\phi_k) + \sqrt{2D}\xi_k(t), \qquad (1)$$

where $k,j=1,2$; $j \neq k$. Natural frequencies of oscillators are $\omega_{1,2}=\omega \pm \Delta/2$, where Δ is the detuning. In Eq. (1), the parameter K is the coupling strength, and $\xi_k(t)$ are zero-mean Gaussian white noise sources with intensities D. The effect of stimuli on oscillators is assumed to be phase dependent [30], and thus modeled by time and phase dependent functions $s_k(t,\phi_k)=X_k(t)\cos(\phi_k)$, where $X_k(t)$ is a pulse $X_k(t)=I_k$, which is on at time t, and $X_k(t)=0$ when the stimulus is off at time t [19].

In the absence of stimuli, $I_k=0$, the dynamics of the phase difference $\psi(t)=\phi_1(t)-\phi_2(t)$ is governed by Adler's equation [31]

$$\dot{\psi} = \Delta - K\sin\psi + \eta(t), \qquad (2)$$

$\eta(t)$ is Gaussian white noise. In the absence of noise ($\eta=0$), synchronization occurs when $K>\Delta$, when Eq. (2) possesses stable and unstable equilibria. Stable equilibrium corresponds to oscillators' phase locking. In the presence of noise, the dynamics of the phase difference can be represented as a motion of a Brownian particle with coordinate ψ in a tilted periodic potential $U(\psi)=-\Delta\psi-K\cos\psi$ [32]. In the case of weak noise, the phase difference trembles within the potential wells and rarely slips from one potential well to another. The detuning Δ determines the tilt of the potential. In the case $\Delta=0$ (identical oscillators), the potential $U(\psi)$ is not tilted and the phase difference slips to the right or to the left from a potential well with equal probabilities. Inhomogeneity of oscillators breaks this symmetry, resulting in a preferred direction of the phase slippage.

B. Stochastic phase resetting analysis

We now consider rectangular stimuli administered to both oscillators, repeatedly at random times t_n, $n=1,\ldots,N$, where N is the number of stimuli administered. The magnitude of pulses is assumed to be significantly larger than the coupling strength K, such that they rapidly reset the oscillators' phases. To extract transient phase responses that are stereotyped and tightly time locked to the stimuli, we perform a cross-trial analysis [19–21]. For this, a time window of width w centered at t_n is attached to every stimulus pulse. An ensemble of oscillators responses is then created by aligning stimulus windows. In each trial window, the stimulus onset is at $t=0$ and $t\in[t_n-w/2,\ t_n+w/2]$. The width of the trial window is assumed to be large compared to both the stimulation duration and transients in oscillators. Equivalently, we can consider an ensemble of N pairs of coupled oscillators subjected to a common stimulus delivered at time $t=0$. Note that there are two sources of randomness in the system. Although the pairs of oscillators are identical, they start with random initial conditions at $t_0=-w/2$ and are subjected to noise sources, which are statistically independent in each oscillator.

Transient statistical properties of the ensemble of responses can be derived from the time-dependent cross-trial probability distributions of the oscillators' phase difference $p(t,\psi)$, and of the oscillators' phases $P_j(t,\phi_j)$ relative to stimuli [19–21]. Valuable information on the extent of stimulus locking can be extracted using absolute values of time-dependent Fourier coefficients of these distributions [19],

$$\lambda_j^{(\nu)}(t) = |\langle \exp[i\nu\phi_j(t)]\rangle|, \quad \sigma(t) = |\langle \exp[i\psi(t)]\rangle|, \qquad (3)$$

where ν is the harmonic number, and brackets $\langle\ldots\rangle$ denote averaging over multiple stimulus trials, here and in the following. One such Fourier coefficient is the *resetting index*

$$\rho_j(t) = \lambda_j^{(1)}(t), \tag{4}$$

which measures whether the phase ϕ_j of the jth oscillator is tightly time locked at time t relative to stimulus onset, across trials. $\rho_j(t)=1$ signifies a perfect reset of the phase of the jth oscillator at time t, such that all stimulus trials lead to exactly the same value of the oscillator's phase. $\rho_j(t)=0$ indicates the absence of resetting. A situation where the phase distribution of the jth oscillator has two antiphase peaks reflects a clustering of the oscillator's responses across trials, which can be quantified by the *clustering index* [20],

$$\alpha_j(t) = \lambda_j^{(2)}(t) - \lambda_j^{(1)}(t). \tag{5}$$

This assumes the value $\alpha_j(t)=1$ if the phase distribution at time t across trials has two Dirac-type symmetric antiphase peaks, corresponding to two clusters of antiphase phase responses of equal size.

The index $\sigma(t)$ quantifies the degree of stimulus-locked synchronization between different oscillators, which can range from 0 to 1. Perfect synchronization corresponds to $\sigma=1$ and means that in all trials we observe the same phase difference at time t relative to stimulus onset, irrespective of the actual value of the phase difference. The absence of synchronization, $\sigma=0$, means that across trials there is no preferred value of the phase difference at time t relative to stimulus onset.

C. Transient dynamics

As a demonstration of the application of stochastic phase resetting analysis, we consider the transient dynamics of two coupled phase oscillators initially synchronized in antiphase. Figure 1 shows the dynamics of an ensemble of 200 transient responses. At a given moment of time, the state of the response ensemble can be displayed as a collection of points on the reference circle [Fig. 1(a)], where the position of a point refers to the phase of a trial at time t. Such a collection of points represents the cross-trial distribution of the phase of an oscillator.

Before stimulation, $t<0$, the oscillators are synchronized in antiphase. Due to the random administration of stimuli, the cross-trial distributions of the oscillators' phases $P_{1,2}(t,\phi_{1,2})$ are uniform [Fig. 1(b)], and the phases of individual trials are uniformly distributed on the reference circle [Fig. 1(a1)]. Correspondingly, the resetting and clustering index vanish in the prestimulus region [Figs. 1(c) and 1(d)]. The cross-trial distribution of the phase difference [Fig. 1(e)] is sharply peaked at $\psi_S=\pi$, giving a synchronization index σ close to 1 [Fig. 1(f)].

Strong identical pulses simultaneously administered to both oscillators quickly reset their phases, such that the phases of all trials are clustered at a particular angle on the reference circle [Fig. 1(a2)]. Correspondingly, the cross-trial distributions of phases are sharply peaked [Fig. 1(b)], giving the resetting indices ρ close to 1 [Fig. 1(c)]. Due to this reset, the oscillators undergo a quick transition from antiphase synchronization to strong in-phase synchrony via a short desynchronization segment, indicated by a trough of the synchronization index in Fig. 1(f). For a short period of time, which

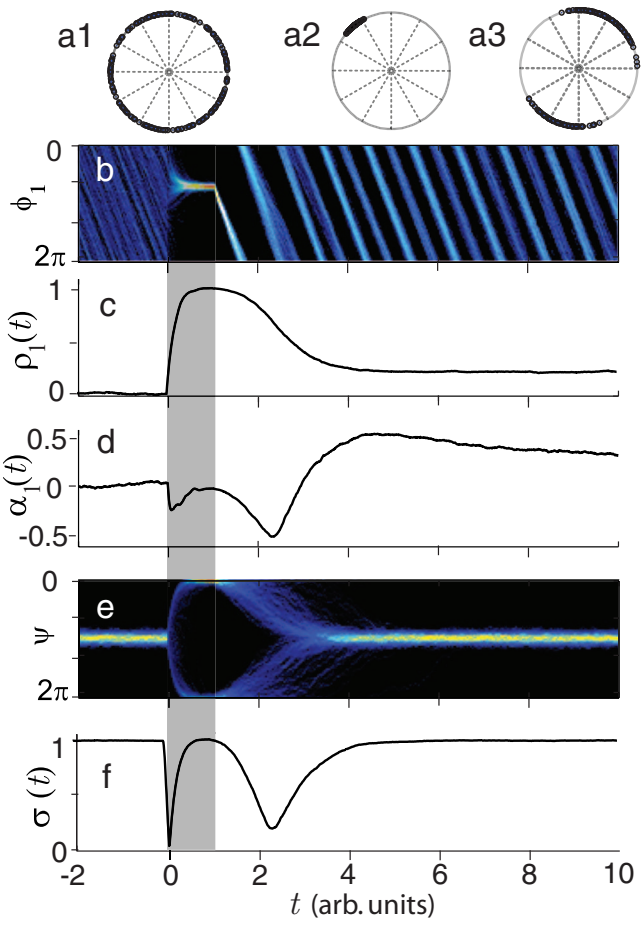

FIG. 1. (Color) Transient dynamics of two coupled phase oscillators Eq. (1) stimulated by 200 rectangular pulses for the case of antiphase synchronization. Stimuli to the two oscillators are shown as a gray vertical bar. Time axis is in units of oscillator periods. The system was simulated for the following parameter values: $\omega=6\pi$, $\Delta=0.2$, $K=-6$, $D=0.1$, $I_1=I_2=30$. The stimulus width is one period. The width of the trial window is $w=60$ periods. [(a)–(d)] Data for oscillator 1 only. (a) Responses of first oscillator displayed on the reference circle for three moments of time: (a1) prestimulus segment, $t=-2$; (a2) at stimulus offset, $t=1$; (a3) poststimulus segment $t=4.31$, corresponding to the maximal value of the clustering index. (b) Cross-trial distribution of the phase of oscillator 1. Low values are indicated by blue, high values by red, and zero by black. (c) Resetting index for oscillator 1. (d) Clustering index for oscillator 1. (e) Cross-trial distribution of the phase difference. (f) Synchronization index.

is determined by the duration of the stimulus, the phase difference is maintained at its unstable equilibrium $\psi=0,2\pi$, e.g., at the top of the potential $U(\psi)$.

In the *poststimulus segment*, the oscillators relax back to the stable state of antiphase synchrony. However, since the system was placed near the unstable equilibrium, there is an uncertainty: relaxation can occur either to the left or to the right wells of the potential $U(\psi)$. Thus, each oscillator begins to form clusters of two alternate paths they can follow while reinstating the stable state of antiphase synchronization. In the particular situation shown in Fig. 1 the selection of the two pathways corresponds to $\phi_1-\phi_2>0$ and $\phi_2-\phi_1>0$,

where $\psi=0$ represents a saddle point of in-phase synchrony. This effect is clearly seen in the reference circle [Fig. 1(a)] as a formation of two separate clusters of responses. The cross-trial probability distributions of the phases are double peaked, indicated by the double stripes in Fig. 1(b). These transient dynamics are well captured by the clustering index [Fig. 1(d)], which becomes positive. While the first brief desynchronization epoch is dictated mainly by the external stimuli, the clustering of oscillator responses is due solely to their interaction, i.e., coupling. This results in an extended desynchronization transient which can last for many periods of oscillations. The clusters of responses persist even after antiphase synchronization is reestablished, and their decay is determined by the noise in the system [20]. In order to obtain an antiphase reset for in-phase synchronized oscillators, the stimuli applied to the oscillators have to be 180° phase shifted [19,21].

Inhomogeneities in the oscillators' parameters, such as detuning of the oscillators' natural frequencies or differences in magnitudes of applied stimuli, result in a degradation of the response clustering effect [20]. For example, frequency detuning results in a tilt of the potential $U(\psi)$, and thus in a preferred direction of poststimulus relaxation to one of the potential wells. On the other hand, asymmetry in stimulus intensities may result in placing the phase difference away from the unstable point, which again leads to a directed flow of poststimulus phase trajectories. A similar effect occurs when the stimuli are delivered with a delay, resulting in a nonantiphase reset [21]. An analytical treatment of inhomogeneity effects is given in the Appendix.

The effect of the relative size of coupling, stimulus strength, and noise on the response clustering was studied in detail in [20,21]. The height of the barrier of the potential $U(\psi)$ is proportional to the coupling strength. Thus, for weak coupling the potential profile becomes shallow and no branching of the phase difference trajectories occurs. As shown in the Appendix, the relaxation time of the resynchronization decreases with the increase of the coupling strength. In the case of detuned oscillators a large coupling results in a fast accumulation of the phase difference responses in a deeper potential well and, thus, no clustering of the absolute phases occurs [21].

Noise has a crucial effect on the transient resynchronization and clustering as studied in [20,21]. In particular, for homogeneous oscillators in the absence of noise, $D=0$, the clusters of absolute phase responses do not decay, while the phase difference relaxes back to the original synchronous state dictated by the coupling. On the other hand, for large noise, the branching of the phase difference trajectories is still observed resulting in the second desynchronization region for the synchronization index. However, coherence of the absolute phase responses, measured by the clustering index, is destroyed by large noise, such that no clustering of absolute phases occurs. Effects of detuning, however, can be compensated by a moderate noise, which causes a symmetric response clustering also in detuned oscillators, as demonstrated in Fig. 1.

It is important to stress that traditional measures for cross-trial analysis, which merely use cross-trial averages of oscillator wave forms, do not capture the clustering dynamics and may even lead to erroneous interpretation of experimental results, as discussed in [19]. In the next section, we analyze the transient dynamics of coupled neuronal bursters using standard peristimulus-type analysis, and compare it to an analysis based on stochastic phase resetting, described above.

III. PADDLEFISH ELECTRORECEPTORS AND EXPERIMENTAL METHODS

We carried out neurophysiological experiments on *in vivo* preparations of paddlefish electroreceptors (ERs) [33]. Electrosense is used for prey capture in this fish, which has an elongated, flattened antennal appendage, the "rostrum," covered with thousands of ERs, extending forward of the head. A single electroreceptor "system" is composed of a cluster of 3–35 skin pores, each leading into a short canal, which terminates in a sensory epithelium containing approximately 400 sensory hair cells [34]. The electrosensitive hair cells of the cluster make excitatory chemical synapses onto the terminals of a few (2–5) primary afferent sensory neurons whose axons project to the brain. ERs are characterized by quasiperiodic spontaneous afferent firing with average frequencies in the range 30–70 Hz, and possess different sensitivity and variability [33]. Individual ERs are not coupled [33,35], forming a parallel sensory array.

ERs have well-defined receptive fields (RFs) on the rostrum, which may be up to 15 cm apart. This allows for nonoverlapping, natural, and noninvasive stimulation of different ERs by presenting weak external time-varying voltage gradients from local dipole electrodes placed near the RFs, controlled by a computer interface. Electric-field stimuli applied to the RF of an electroreceptor may significantly alter its quasiperiodic tonic patterns of afferent firing [33]. For example, inhibitory stimuli of large enough magnitude may drive afferent neurons to a quiescence regime in which they stop firing.

Although the afferents of different ERs fire continuously at different rates and typically differ in sensitivity and variability, they share a common slow time scale of stimulus-evoked bursting [35]. A time-dependent stimulus may result in a bursting mode, where spikes are grouped in clusters or bursts, which are separated by prolonged quiescence epochs of no firing. Bursting dynamics were also observed when ERs were chilled to 4–7 °C [33].

A. Experimental methods

Figure 2 shows the experimental setup for creating a hybrid neuroelectronic system. Simultaneous recordings of afferent firing were obtained from two ERs having distant RFs (see [33] for details on electrophysiology). Local stimulation of their RFs was controlled by a programmable interface, model P1401, Cambridge Electronic Devices, and model DS1104, dSpace Inc., operated by a PC.

To obtain slow oscillations in the form of afferent bursts, having similar frequencies, we instituted artificial feedback loops by recording the spike train from an ER afferent, and delivering back to its RF a feedback signal $y(t)$ derived by

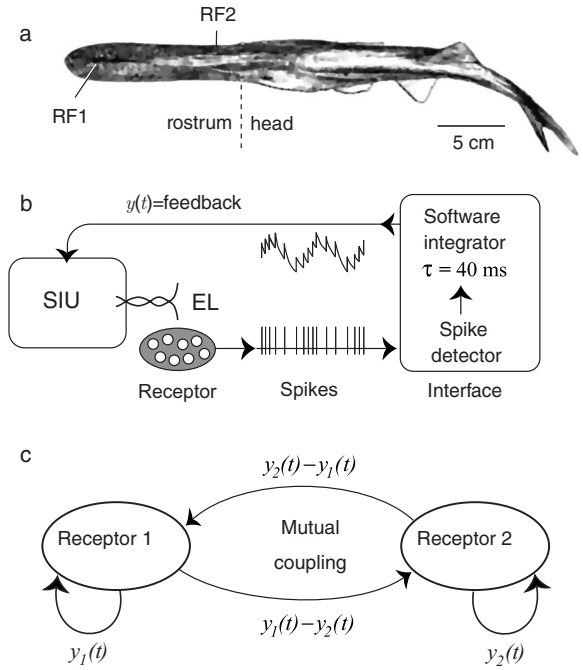

FIG. 2. Experimental setup. (a) Dorsal view of a paddlefish, showing the widely separated receptive fields of two electroreceptors (RF1 and RF2) on the rostrum, used in these experiments. (b) Feedback to a given receptor came from real-time computation (see text). (c) Systems of two coupled bursters, each with a feedback [as in (b)].

converting (in software) its afferent spike train to a continuous wave form, obtained by calculating the instantaneous afferent firing rate, then smoothing it in software using a 40 ms low-pass filter. This convolved signal commanded a linear stimulus isolation unit (SIU) connected to a small dipole stimulating electrode (EL) over the RF.

Positive (excitatory) or negative (inhibitory) feedback could be obtained by inverting the $y(t)$ signal; the strength of feedback was set in software. Feedback resulted in periodic bursting firing of the afferent (Fig. 3). Excitatory feedback gave interburst intervals of ≈ 1 s, while inhibitory feedback, used in the data shown below, resulted in shorter bursts at

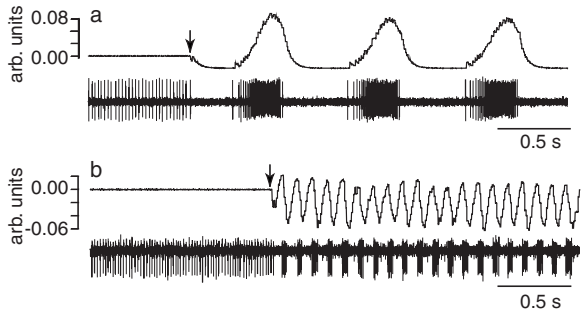

FIG. 3. Afferent bursting due to feedback. The normal tonic afferent firing at ≈ 50 Hz changed promptly to bursting when a feedback loop was closed (indicated by arrows). Panels (a) and (b) correspond to excitatory and inhibitory feedback, respectively. In each panel the lower trace is afferent spikes and the upper trace is the feedback signal $y(t)$, a.u.: arbitrary units.

intervals of ≈ 0.1 s. The delay of the feedback was 10–30 ms and, hence, smaller than the period of bursting.

We also instituted computer-imposed mutual diffusive coupling between the ERs [Fig. 2(c)]. Coupling from ER #2 to ER #1 was computed as the difference $y_2(t)-y_1(t)$, and as $y_1(t)-y_2(t)$ from ER #1 to ER #2, where $y_{1,2}(t)$ are the ERs' smoothed firing rates. These coupling signals were fed to the other receptor with a strength giving robust *synchronization of bursts* [25,28,36]. Depending on the sign of the coupling strength, we obtained either in-phase or antiphase synchronization of bursts.

Rectangular 75 ms phase-resetting stimulus pulses were delivered repeatedly at random times t_k to the RFs receptive fields of both electroreceptors. The stimulus magnitude was 20 times larger than the coupling strength.

B. Data analysis

An ensemble of ER responses to repeated stimuli was created by imposing nonoverlapping "trial" time windows of width $w=2$ s centered at stimulus times t_k, $t \in [t_k - w/2,\ t_k + w/2]$. In each trial window, the stimulus onset is at $t=0$. An ER's spike train within a trial window is defined as $x_j(t) = \sum_{n=1}^{M} \delta(t-\tau_n)$, where τ_n, $n=1,\ldots,M$ are spike times of the jth ER. An analysis approach commonly used in neuroscience to characterize a neuron's responses [37] is the time-dependent spike rate $r_j(t)$ at time t relative to stimulus onset, also known as the peristimulus time histogram (PSTH), defined as $r_j(t) = \langle x_j(t) \rangle$.

To calculate instantaneous phases $\phi_j(t)$ of bursts, the spike trains $x_j(t)$ were first convolved with $s=50$ ms cosine windows,

$$y_j(t) = \frac{1}{2s} \sum_{n=1}^{M} \left[1 + \cos \frac{\pi(t-\tau_n)}{s} \right] \theta(t - \tau_n - s), \qquad (6)$$

where $\theta(t)$ is the Heaviside step function. Then the Hilbert transform [38] was applied to the smoothed signals $y_j(t)$ to estimate $\phi_j(t)$ and the phase difference $\psi(t) = \phi_1(t) - \phi_2(t)$. An alternate approach was to first identify bursts' onsets, and then calculate phases of burst trains using a linear interpolation: the phase of an ER increases by 2π every time a burst occurs and interpolates linearly between two subsequent bursts. Both approaches gave identical results. Cross-trial phase distributions and corresponding indices were calculated as described in Sec. II above.

IV. EXPERIMENTAL RESULTS

Data were from 12 pairs of electroreceptors from six paddlefish. Clear response clustering was observed in three pairs of electroreceptors. Figure 4 shows an example of antiphase synchronized ERs perturbed by identical inhibitory stimuli administered simultaneously to both ERs. ERs were brought to bursting regimes by inhibitory feedback and synchronized in antiphase using diffusive excitatory coupling [39]. Inhibitory stimuli acted to delayed bursts in both ERs, bringing them briefly to in-phase synchrony. After stimulation, the stable antiphase synchrony recovered.

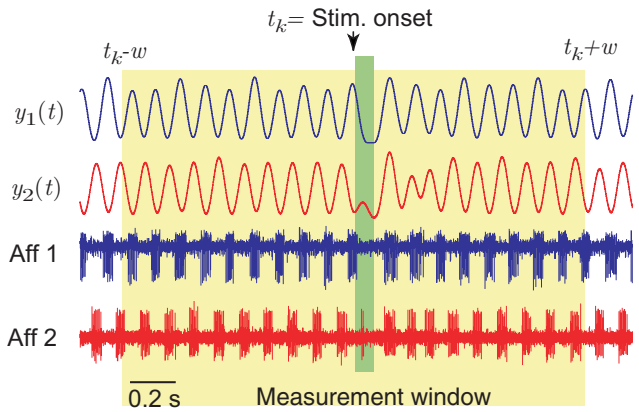

FIG. 4. (Color) Antiphasic synchronized bursts from a mutually coupled two-neuron hybrid model. Lower traces: raw spike trains. Upper traces: feedback signals $y_1(t)$ and $y_2(t)$. Vertical green bar: 75 ms square-wave inhibitory stimulus to both electroreceptors. Yellow background: one measurement window, $w=2$ s.

In the majority of experiments, we used coupling resulting in antiphase synchronization of bursts, for the following reason. ERs can differ in sensitivity and adaptation properties to excitatory and inhibitory stimuli. Thus, to minimize heterogeneity of neuronal responses, it was advantageous to stimulate ERs with simultaneous stimuli of the same polarity, which tended to synchronize them in phase. Thus, in order to achieve an antiphase reset, the original state of synchronization had to be antiphase. Desynchronization of in-phase synchronized ERs was possible too, but required stimuli of opposite polarity and thus adjustment of stimuli amplitude in order to compensate for differences in gain and adaptation. Alternatively, an antiphase reset was possible with stimuli of the same polarity, administered with a time delay equal to exactly half a period of bursting [21].

A. Comparison of simultaneous vs delayed stimulation

We start with two ERs brought to bursting regimes by inhibitory feedback, and synchronized in antiphase using diffusive excitatory coupling, as described above. First, we perturbed the ERs with a sequence of 88 inhibitory pulses delivered *simultaneously* to the RFs receptive fields of both ERs [Fig. 5(a)], and applied conventional analysis in terms of raster plots and PSTHs. In the prestimulus region, the spikes in both ERs occurred randomly with respect to stimuli onsets, and thus the PSTHs were uniform. Immediately after stimulation, both ERs fired in concert relative to the stimuli, giving rise to a large-amplitude deviation of PSTHs, which then faded away, reflected by a rapid decay of the oscillations in the PSTHs.

Next, the same coupled ERs were perturbed with pulses delivered with a delay, such that ER #2 was stimulated 50 ms after the onset of a stimulus to ER #1 [Fig. 5(b)]. The poststimulus segment differs drastically from the previous case of simultaneous stimulation: the raster plot shows structured alternations of neuronal firing, and PSTHs show large-amplitude slowly-decaying oscillations in the poststimulus segment, clearly indicating that the oscillators' responses

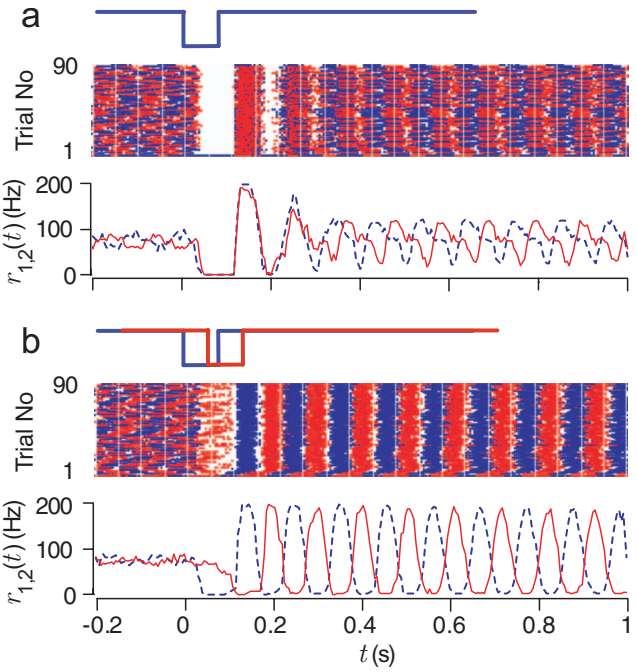

FIG. 5. (Color) Two coupled bursting electroreceptors (ERs) were stimulated with inhibitory pulses in 88 randomly spaced trials. (a) Stimuli were administered simultaneously to both ERs. (b) ER #2 was stimulated 50 ms after ER #1. In both panels, the upper rows show inhibitory stimuli. The middle rows show a raster plot when spikes of ER #1 are indicated by blue dots and spikes in ER #2 by red dots. The lower rows show PSTHs for the two bursting ERs, with corresponding colors: blue dashed line is for ER #1; red solid line is for ER #2.

were almost perfectly locked to the stimuli, even after 10 periods of poststimulus oscillations, with little decay.

Erroneous interpretations of the transient dynamics shown in Fig. 5 could occur if based solely on the PSTHs, or more generally, on simple cross-trial averaging (see also [19]). For example, a possible interpretation of Fig. 5 could be that the two different types of brief stimuli acted to induce oscillatory responses with small [Fig. 5(a)] or large [Fig. 5(b)] amplitudes, despite similar prestimulus firing rates. This interpretation is shown below to be incorrect, because it fails to consider phase information.

To take into account the phase information, we employed the cross-trial phase resetting analysis, shown in Fig. 6 for the case of simultaneous stimulation. In the prestimulus range, the ERs were synchronized in antiphase, that is, near a phase difference of π. Stimuli (vertical bar) reset the phases of both oscillators, bringing them to in-phase synchrony, which persisted briefly after stimulation [asterisk, Fig. 6(a)]. The resetting index $\rho_j(t)$ [Fig. 6(c)] was close to 0 in the prestimulus domain, due to the randomized times of stimulus administration. $\rho_j(t)$ increased rapidly during stimulation to its maximum possible value of 1, indicating a strong reset. Resetting indices then relaxed back to 0 quickly, indicating that the oscillators promptly "forgot" their new reset phases. In the course of the reset, the synchronization index $\sigma(t)$ [Fig. 6(d)] showed *two* desynchronization segments: the value of $\sigma(t)$ temporarily fell (detecting a transient desyn-

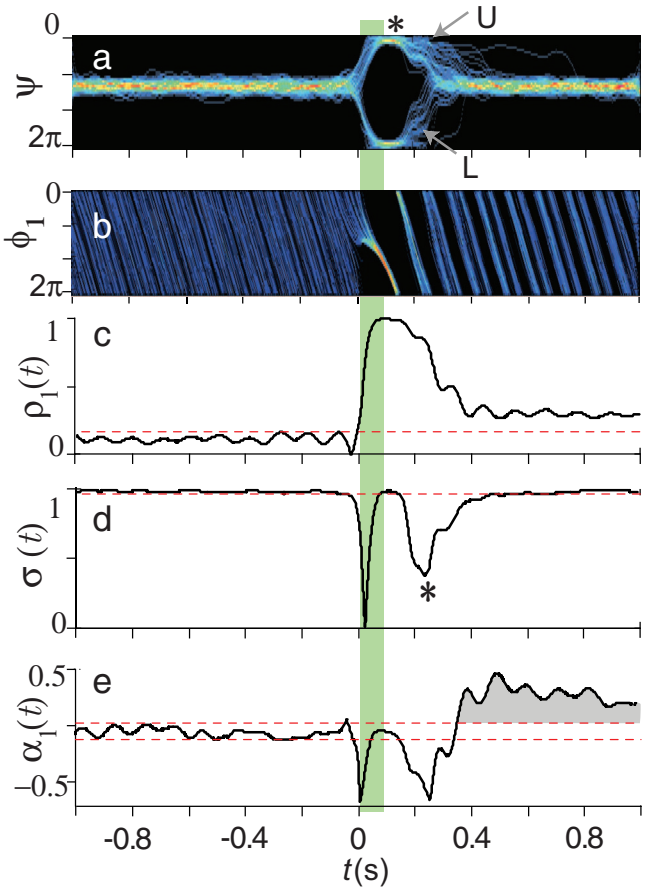

FIG. 6. (Color) Transient phase dynamics after simultaneous 75 ms inhibitory stimulation of a network of two electroreceptor bursters, each with inhibitory feedback and excitatory mutual coupling, as in Fig. 4. The stimuli, at random times, are indicated by a vertical bar at $t=0$ across panels (a)–(e). (a) Time-dependent probability density of the phase difference of the two bursters. Low values are indicated by blue, high values by red, and zero by black. Arrows show upper (U) and lower (L) branches of trial trajectories (see text). (b) Time-dependent probability density of the phase of burster #1, relative to the onsets of stimuli. Note double-peaked structures in the poststimulus domain, denoted as blue bands separated by narrow black stripes. (c) Time course of resetting index for burster #1. The dashed line indicates the significance level at the 99th percentile of the prestimulus ($t<0$) distribution. (d) Time course of synchronization index. (e) Time course of clustering index for burster #1. The shaded area indicates a statistically significant epoch of clustering.

chronization) during the stimulus at the transition from antiphase to in-phase synchronization, and again later when the temporary poststimulus state of in-phase synchronization decayed [asterisk, Fig. 6(d)]. These results illustrate the usefulness and effectiveness of the resetting and synchronization indexes for characterizing transient phase dynamics in experimental data.

B. Response clustering

During the second, poststimulus, more extended epoch of oscillator desynchronization [asterisk, in Fig. 6(d) (asterisk)],

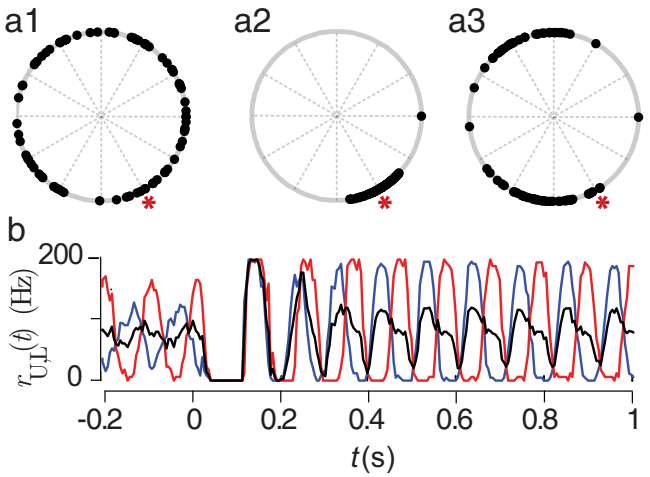

FIG. 7. (Color) Response clustering. (a) Responses of burster #1 displayed on the reference circle for three moments of time relative to the stimulus onset. (a1) In the prestimulus segment ($t=-1$ s), points were distributed uniformly on the reference circle. (a2) Shortly after the offset of the stimulus when the resetting index reached its maximal value ($t=0.137$ s), the phase of burster #1 was reset across trials, and thus points on the reference circle were concentrated within a single cluster. (a3) In the poststimulus segment, the trail responses formed two clusters while the clustering index reached its maximal value at $t=0.505$ s. The red asterisks indicate the phase of burst onsets. (b) Selective PSTHs of the two branched responses of burster #1. The red and blue lines show PSTHs for upper (U) and lower (L) branches of Fig. 6(b). The black line shows PSTH for the whole ensemble of burster #1 trials [same as the blue dashed line in Fig. 5(a)].

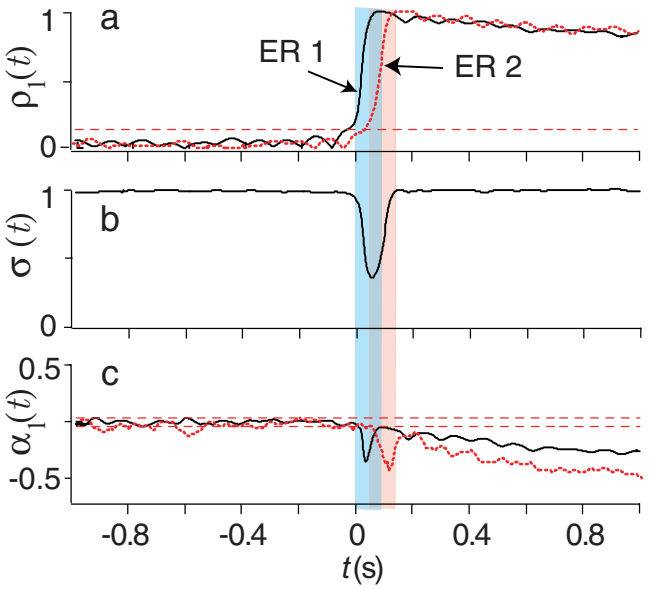

FIG. 8. (Color) Transient dynamics of coupled electroreceptors in the case when ER #2 was stimulated 50 ms after ER #1. The stimuli to ER #1 and ER #2 are indicated by blue and pink vertical bars, respectively. In (a)–(c), solid black lines refer to ER #1 and dotted red lines refer to ER #2. (a) Time course of resetting index. (b) Time course of clustering index. (c) Time course of synchronization index. The dashed line indicates a significance level at the 99th percentile of the prestimulus ($t<0$) distribution.

the trial responses of each oscillator began to form clusters of two alternate phase trajectories, which they could follow while relaxing back to the usual antiphase synchronization, from the transient poststimulus epoch of in-phase synchronization. The alternate paths are seen as a lower (L) or upper (U) branch of the oscillators' phase difference [Fig. 6(a)]. Formation of the response clusters is also seen as double peaks in the distributions of each oscillator's phase relative to stimuli $P_j(t,\phi_j)$, shown in Fig. 6(b) for ER #1, and is clearly displayed on the reference circle [Fig. 7(a3)]. To resynchronize in antiphase, either ER #1 had to fall behind ER #2, or vice versa; these alternatives correspond to the two branches of the poststimulus desynchronization segment, seen as two clusters on the reference circle. Such clusters persisted >10 cycles after reinstatement of antiphase synchronization.

Clustering was quantified as significantly positive values of the clustering index $\alpha_j(t)$. In Fig. 6(e), the maximum of $\alpha_j(t)$ (gray shading), when it was significantly above the prestimulus baseline range, indicates when the most pronounced double-peaked structure of $P_j(t,\phi_j)$ occurred. The subsequent decline of $\alpha_j(t)$ was due to noise in the system [20].

Clustering could also be revealed in PSTHs for a given oscillator, by separately grouping the trials leading to the upper (U) or lower (L) branch of the poststimulus desynchronization segment [arrows, Fig. 6(a)]. The selective PSTHs calculated for each branch [solid red, dashed blue lines, Fig. 7(b)], showed large-amplitude antiphasic oscillations. They were antiphasic because of the two different ways to reestablish antiphase synchronization after stimulation (that is, ER #1 falls behind ER #2, or vice versa). In contrast, the PSTH of the whole ensemble of trials [black dotted line, Fig. 7(b)] showed smaller-amplitude oscillations, because it was the mean of the antiphasic selective PSTHs, which canceled. Thus, a relatively uniform ensemble PSTH may not signify that the average response of an oscillator is small, but instead may result from cancellation of responses, which are phase shifted in different trials, e.g., due to response clustering.

If stimuli were administered not simultaneously to both receptors, but instead with a significant delay [as in Fig. 5(b)], the response clustering did not occur. Delayed stimuli induced long-lived (>10 cycles) elevation of the resetting index, shown in Fig. 8(a). However, the two oscillators became desynchronized only briefly, during stimulation [Fig. 8(b)]. The clustering index never reached a significantly positive level [Fig. 8(c)], consistent with there not being any poststimulus epoch of unstable in-phase synchrony. In general, unstable synchronization is required to observe alternate phase trajectories (that is, response clustering) during relaxation to a stable phase relation of the oscillators.

V. CONCLUSION

We revealed response clustering in a hybrid neuroelectronic system of two coupled paddlefish electroreceptors. These experimental results are in agreement with the transient dynamics predicted using numerical simulations of a generic phase model for two coupled oscillators. In an ideal symmetric situation of two identical oscillators, synchronized in antiphase, a stimulus-induced reset to in-phase synchronization corresponds to placing the phase difference at the unstable equilibrium state $\phi_u=0,2\pi$. Due to noise, there is uncertainty as to whether an oscillator will relax after a stimulus to one stable state or the other, $\phi_s=\pm\pi$. This uncertainty is the source of the decorrelation of responses. Thus, the unstable state separates the ensemble of responses into two groups, leading to the formation of two clusters, such that the phase distributions of both oscillators $P_{1,2}(t,\phi)$ possess two peaks. The decorrelation of responses resulting from clustering tends to cause cross-trial averaged signals to vanish. Our results emphasize that information about the phases of neuronal oscillators must be retained and utilized in order to correctly interpret and quantify transient stimulus-evoked dynamics, whereas traditional neuroscience metrics based on simple cross-trial averaging, which lose and ignore phase information, may be misleading.

The decorrelation of responses was incomplete in our experimental data, as indicated by small-amplitude poststimulus oscillations of PSTHs in the lower row of Fig. 5(a). Several causes can lead to such an effect [20], including nonidentity of the coupled ER bursters, nonidentity of stimulus intensities, or time-delay effects in propagation of stimulus-induced changes (for example, spike propagation delays from receptive fields to recording sites). The coupling strength also plays a significant role in clustering of oscillators responses. When the coupling strength between the electroreceptors was too strong, the clustering effect disappeared (not shown), as the stimulus was not strong enough to place the bursters at the unstable state. On the other hand, indeed, no clustering occurred in the system of uncoupled electroreceptors, as a control. Some units demonstrated a high degree of variability of the bursting. In terms of the model (1) this corresponded to a large noise intensity D. Although a branching of the phase differences trials was observed, a clustering of the absolute phases was insignificant (not shown), since the large noise rapidly smeared out the response clusters.

Recently, the impact of resetting stimuli on two phase oscillators coupled with delayed self-feedback was investigated [22], which showed that maximal response clustering as well as maximal resynchronization time occur if a system gets trapped at a stable manifold of an unstable saddle fixed point, due to appropriately calibrated stimuli. For this, the two oscillators have to be reset in such a manner that their phase difference attains a value which—for nonvanishing delay—differs from that of the unstable fixed point. The emergence of long resynchronization transients is a consequence of the delayed component in the coupling term [22]. Since coupling delays are inevitable in biological systems, it might be interesting to study whether it is possible to exploit the impact of coupling delays for control purposes, e.g., by causing long resynchronization transients by appropriately timed resetting stimuli.

The experimental system that we used, consisting of two electroreceptors of paddlefish, coupled externally and stimulated naturally and noninvasively, makes use of real neurons yet is relatively well defined. ERs offer a natural interface with electronics, since their sensory modality is the detection

of weak voltage gradients, and their responses are proportional to stimulus strength (graded) and are dual polarity (inhibited or excited per stimulus electrical polarity). This experimental model's neurons includes complex processes such as excitatory synaptic transmission from receptor cells to afferents, and adaptation, and internal higher-frequency oscillations [33]. Thus, our experimental results and analytical studies are of interest for characterizing the transient dynamics of other complex systems, including other neural systems.

ACKNOWLEDGMENTS

Experiments were done at the Center for Neurodynamics, University of Missouri at St. Louis. This work was supported by the U.S. National Institute on Deafness and Other Communication Disorders (Grant No. DC-04922), the U.S. National Science Foundation (Grant No.INT-0233264), the EU Network of Excellence in Biosimulation (BioSim—LSHB—CT—20004– 005137), the German Israeli Foundation, the German Academic Exchange Service, and by IBM. We thank P. Jung and F. Moss for discussions and comments.

APPENDIX: ANALYTICAL TREATMENT OF RESPONSE CLUSTERING

The analytical treatment of Eq. (1) is hampered by a requirement for a time-dependent solution of the corresponding two-dimensional Fokker-Planck equation. However, the effects of asymmetries can be studied analytically by separately considering the prestimulus, during stimulus, and poststimulus segments, in the limit of large coupling and strong stimulus, when noise can be neglected.

In the *prestimulus region* $t<0$ the dynamics of the system are governed by Adler's Eq. (2). We consider the case of strong synchronization, $|K|\gg\Delta$ and $|K|\gg D$, so that no phase slippage occurs and noise can be neglected. The phase difference is constant, $\psi(t<0)=\psi_S=\arcsin(\Delta/K)$. The oscillators' phases $\phi_{1,2}$ are uniformly distributed across trials due to the random administration of the stimuli.

At stimulus onset $(t=0)$, the phases of both oscillators are uniformly distributed across trials. Since both oscillators are synchronized, the phase difference at $t=0$ is fixed at $\psi(0)=\psi_S$ and thus, the random phases $\phi_{1,2}(0)$ are coupled according to $\phi_1(0)-\phi_2(0)=\psi_S$.

During stimulation, $0<t\le\tau_s$ (τ_s is the duration of the stimulus), we assume $I_k\gg|K|$ and neglect both coupling and noise in Eq. (1), since $I_k\gg|K|$ and $I_k\gg D$. This provides us with a simplified equation for the phases of the oscillators, $\dot{\phi}_k=\omega_k+I_k\cos\phi_k$, which can be easily solved with the initial conditions $\phi_1(0)=\phi_0$ and $\phi_2(0)=\phi_0-\psi_S$,

$$\phi_k(t,\phi_k(0))=2\arctan\left[\frac{1}{\alpha_k}\frac{e^{\beta_k t}-B_k(\phi_k(0))}{e^{\beta_k t}+B_k(\phi_k(0))}\right],$$

$$\alpha_k=\left(\frac{I_k-\omega_k}{I_k+\omega_k}\right)^{1/2},\quad \beta_k=(I_k^2-\omega_k^2)^{1/2},$$

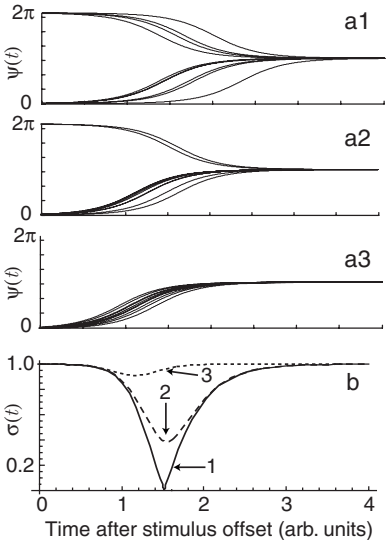

FIG. 9. Poststimulus segment of the transient dynamics of two coupled phase oscillators calculated analytically according to Eqs. (10) and (11). The parameters are $\omega_1=\omega_2=6\pi$, $K=-3$, $I_1=30$. (a) Ten trajectories of the phase difference were calculated according to Eq. (10). Initial phase differences ψ_p were uniformly distributed in $[\psi_R-d/2\psi_R+d/2]$, $d=0.1$. Three panels [(a1)–(a3)] correspond to different values of the stimulus magnitude of the second oscillator, $I_2=30$ (a1); $I_2=31$ (a2); $I_2=33$ (a3). (b) Poststimulus time course of the synchronization index Eq. (11). Three curves correspond to the values of I_2 in the panel (a): $I_2=30$ (solid line 1); $I_2=31$ (dashed line 2); $I_2=33$ (dotted line 3).

$$B_k(x)=\frac{1-\alpha_k\tan\frac{x}{2}}{1+\alpha_k\tan\frac{x}{2}},\quad I_k>\omega_k,\quad 0\le t\le\tau_s. \tag{A1}$$

Equation (A1) gives the phase trajectories of the trial responses with the *random* initial condition ϕ_0 drawn from a uniform distribution, $P(\phi_0)=1/2\pi$, $\phi_0\in[0\ 2\pi)$. The trial responses relax to the equilibrium reset values $\pi-\arccos(\omega_k/I_k)$, with the characteristic time determined by the constants β_k. In the case of identical oscillators synchronized in antiphase and identical stimuli, the phase difference is reset to $\psi_R=0$, that is, to the unstable equilibrium of Adler's equation. However, detuning of the oscillators and/or a difference in stimulus magnitudes shift the reset value of the phase difference away from the unstable point,

$$\psi_R=\arccos(\omega_2/I_2)-\arccos(\omega_1/I_1). \tag{A2}$$

The Fourier coefficients (3) can be calculated by averaging across the ensemble of initial phases ϕ_0. In the thermodynamic limit of infinitely many trials, we have $\lambda_k^{(\nu)}=1/(2\pi)\left|\int_0^{2\pi}\exp[i\nu\phi_k(t,\phi_0)]d\phi_0\right|$. In the limit $I_k\gg\omega_k$, we obtain simple expressions for the resetting and synchronization indices,

$$\rho(t)=\tanh\left(\frac{It}{2}\right),\quad \sigma(t)=|1-2\ \mathrm{sech}(It)|,\quad 0\le t\le\tau_s. \tag{A3}$$

The poststimulus segment $t > \tau_s$ can be analyzed using Adler's Eq. (2). In the limit $|K| \gg D$, we again neglect noise, but assume that at stimulus offset the phase difference $\psi(\tau_s) = \psi_p$ is a random variable distributed around ψ_R. For simplicity, we consider a narrow uniform distribution with the width d centered at ψ_R, and identical oscillators $\Delta = 0$. The solution of Adler's equation with the initial condition $\psi(\tau_s) = \psi_p$ takes a simple form,

$$\psi(t, \psi_p) = 2 \arctan\left[e^{-K(t-\tau_s)} \tan\frac{\psi_p}{2} \right], \quad t \geq \tau_s. \tag{A4}$$

For a given initial phase difference ψ_p, the characteristic relaxation time is determined by the coupling strength K. The synchronization index (3) can be calculated in the thermodynamic limit as

$$\sigma(t) = \frac{1}{d} \left| \int_{\psi_R - d/2}^{\psi_R + d/2} \exp(i\psi(t, \psi_p)) d\psi_p \right|, \tag{A5}$$

and is shown in Fig. 9. In the case of identical stimuli $I_1 = I_2$ the distribution of the initial phase differences is centered at $\psi_R = 0$. This unstable point separates transients into two symmetric paths [Fig. 9(a1)]. At $t \approx 1.5$, the synchronization index drops to zero due to the symmetric splitting of the trial responses into two antiphase clusters [curve 1 in Fig. 9(b)]. In the case of nonidentical stimuli, the splitting of the trial responses becomes asymmetric [Fig. 9(a2)], indicated by a nonvanishing minimum of the synchronization index [curve 2 in Fig. 9(b)]. For a larger mismatch of the stimuli, the splitting of the trial responses no longer occurs [Fig. 9(a3)], and the effects of clustering and poststimulus desynchronization disappear [curve 3 in Fig. 9(b)].

[1] A. Pikovsky, M. Rosenblum, and J. Kurths, *Synchronization: A Universal Concept in Nonlinear Science* (Cambridge University Press, Cambridge, England, 2003).
[2] L. Glass, Nature **410**, 277 (2001).
[3] G. Laurent, Trends Neurosci. **19**, 489 (1996).
[4] K. MacLeod and G. Laurent, Science **274**, 976 (1996).
[5] W. Singer and C. M. Gray, Annu. Rev. Neurosci. **18**, 555 (1995).
[6] J. J. Hopfield and C. D. Brody, Proc. Natl. Acad. Sci. U.S.A. **98**, 1282 (2001).
[7] M. B. Zugaro, L. Moconduit, and G. Buzsaki, Nat. Neurosci. **8**, 67 (2005).
[8] I. Hertrich, K. Mathiak, W. Lutzenberger, and H. Ackermann, Neuroreport **15**, 1687 (2004).
[9] S. Makeig *et al.*, Science **295**, 690 (2002); K. Kirschfeld, Biol. Cybern. **92**, 177 (2005); B. Ross *et al.*, J. Neurophysiol. **94**, 4082 (2005); A. Mazaheri and O. Jensen, Proc. Natl. Acad. Sci. U.S.A. **103**, 2948 (2006); W. Klimesch *et al.*, Neuroimage **29**, 808 (2006); S. Hanslmayr *et al.*, Cereb. Cortex **17**, 1 (2007).
[10] A. Nini, A. Feingold, H. Slovin, and H. Bergman, J. Neurophysiol. **74**, 1800 (1995).
[11] H. Bergman *et al.*, Trends Neurosci. **21**, 32 (1998).
[12] J. M. Hurtado, L. I. Rubchinsky, K. A. Sigvardt, V. I. Wheelock, and C. T. Pappas, J. Neurophysiol. **93**, 1569 (2005).
[13] A. L. Benabid *et al.*, Lancet **337**, 403 (1991).
[14] P. A. Tass, *Phase Resetting in Medicine and Biology: Stochastic Modelling and Data Analysis* (Springer Verlag, Berlin, 1999).
[15] P. A. Tass, Biol. Cybern. **87**, 102 (2002); **89**, 81 (2003).
[16] M. G. Rosenblum and A. S. Pikovsky, Phys. Rev. Lett. **92**, 114102 (2004).
[17] O. V. Popovych, C. Hauptmann, and P. A. Tass, Phys. Rev. Lett. **94**, 164102 (2005).
[18] P. A. Tass, C. Hauptmann, and O. V. Popovych, Int. J. Bifurcation Chaos Appl. Sci. Eng. (to be published).
[19] P. A. Tass, Europhys. Lett. **59**, 199 (2002).
[20] P. A. Tass, Chaos **13**, 364 (2003).
[21] P. A. Tass, Phys. Rev. E **67**, 051902 (2003).
[22] V. Krachkovskyi, O. V. Popovych, and P. A. Tass, Phys. Rev. E **73**, 066220 (2006).
[23] Y. Kuramoto, *Chemical Oscillations, Waves, and Turbulence* (Springer-Verlag, Berlin, 1984).
[24] A. J. Preyer and R. J. Butera, Phys. Rev. Lett. **95**, 138103 (2005).
[25] E. M. Izhikevich, Int. J. Bifurcation Chaos Appl. Sci. Eng. **10**, 1171 (2000).
[26] H. Bergman, T. Wichmann, B. Karmon, and M. R. DeLong, J. Neurophysiol. **72**, 507 (1994).
[27] I. Raikov, A. Preyer, and R. J. Butera, J. Neurosci. Methods **132**, 109 (2004).
[28] R. C. Elson, A. I. Selverson, R. Huerta, N. F. Rulkov, M. I. Rabinovich, and H. D. I. Abarbanel, Phys. Rev. Lett. **81**, 5692 (1998).
[29] P. Varona, J. J. Torres, H. D. Abarbanel, M. I. Rabinovich, and R. C. Elson, Biol. Cybern. **84**, 91 (2001).
[30] A. T. Winfree, *The Geometry of Biological Time* (Springer, Berlin, 1980).
[31] R. Adler, Proc. IRE **34**, 351 (1946).
[32] R. L. Stratonovich, *Theory of Random Noise* (Gordon and Breach, New York, 1964), Vols. I and II.
[33] A. B. Neiman and D. F. Russell, J. Neurophysiol. **92**, 492 (2004).
[34] J. M. Jørgensen, Å. Flock, and J. Wersäll, Z. Zellforsch. Mikrosk. Anat. **130**, 362 (1972).
[35] A. B. Neiman and D. F. Russell, Phys. Rev. Lett. **88**, 138103 (2002).
[36] T. I. Netoff and S. J. Schiff, J. Neurosci. **22**, 7297 (2002).
[37] C. Koch, *Biophysics of Computations* (Oxford University Press, New York, 1999).
[38] M. G. Rosenblum, A. S. Pikovsky, and J. Kurths, Phys. Rev. Lett. **76**, 1804 (1996).
[39] A. Sherman and J. Rinzel, Proc. Natl. Acad. Sci. U.S.A. **89**, 2471 (1992).